

Direct Parameterization of Lipschitz-Bounded Deep Networks

Ruigang Wang¹ Ian Manchester¹

Abstract

This paper introduces a new parameterization of deep neural networks (both fully-connected and convolutional) with guaranteed Lipschitz bounds, i.e. limited sensitivity to perturbations. The Lipschitz guarantees are equivalent to the tightest-known bounds based on certification via a semidefinite program (SDP), which does not scale to large models. In contrast to the SDP approach, we provide a “direct” parameterization, i.e. a smooth mapping from \mathbb{R}^N onto the set of weights of Lipschitz-bounded networks. This enables training via standard gradient methods, without any computationally intensive projections or barrier terms. The new parameterization can equivalently be thought of as either a new layer type (the *sandwich layer*), or a novel parameterization of standard feedforward networks with parameter sharing between neighbouring layers. Finally, the comprehensive set of experiments on image classification shows that sandwich layers outperform previous approaches on both empirical and certified robust accuracy.

1. Introduction

Neural networks have enjoyed wide application due to their many favourable properties, including highly accurate fits to training data, surprising generalisation performance within a distribution, and well as scalability to very large models and data sets. Nevertheless, it has also been observed that they can be highly sensitive to small input perturbations (Szegedy et al., 2014). This is a critical limitation in applications in which certifiable robustness is required, or the smoothness of a learned function is important.

A standard way to quantify sensitivity of a models is via

¹Australian Centre for Robotics, School of Aerospace, Mechanical and Mechatronic Engineering, The University of Sydney, Sydney, Australia. Correspondence to: Ruigang Wang <ruigang.wang@sydney.edu.au>.

a *Lipschitz bound*, which generalises the notion of a slope-restricted scalar function. A learned function $x \mapsto f(x)$ between normed spaces satisfies a Lipschitz bound γ if

$$\|f(x_1) - f(x_2)\| \leq \gamma \|x_1 - x_2\|$$

for all x_1, x_2 in its domain. The (true) Lipschitz constant of a function, denoted by $\text{Lip}(f)$, is the smallest such γ .

A natural application of Lipschitz-bounds is to control a model’s sensitivity *adversarial* (worst-case) inputs, e.g. (Madry et al., 2018; Tsuzuku et al., 2018), but Lipschitz constants also appear in bounds on statistical generalisation performance (Bartlett et al., 2017). Lipschitz-bounds have been applied to help stabilise the learning of generative adversarial networks (Arjovsky et al., 2017; Gulrajani et al., 2017), and more recently in implicit geometry mechanisms for computer graphics (Liu et al., 2022). Lipschitz-bounded networks have also been investigated in the context of reinforcement learning and control problems, for controlling sensitivity to measurement noise (e.g. (Russo & Proutiere, 2021)) and ensuring robust stability of feedback loops during training (Wang & Manchester, 2022). In robotics applications, several learning-based planning and control algorithms require known Lipschitz bounds in learned stability certificates, see e.g. the recent surveys (Brunke et al., 2022; Dawson et al., 2023).

Unfortunately, even for two-layer perceptions with ReLU activations, exact calculation of the true Lipschitz constant for ℓ^2 (Euclidean) norms is NP-hard (Virmaux & Scaman, 2018), so attention has focused on approximations that balance accuracy with computational tractability. For ℓ^1 and ℓ^∞ norms, simple Lipschitz bounds can be expressed in terms of row and column sums of layer weights (Gouk et al., 2021), but for ℓ^2 it is more complex. Crude bounds can be found via the product of spectral norms of layer weights (Szegedy et al., 2014), however to date the most accurate bounds require solution of a semidefinite program (SDP) (Fazlyab et al., 2019), which is computationally tractable only for relatively small fully-connected networks.

Furthermore, while *certification* of a Lipschitz bound of a fixed network is a (convex) SDP with this method, the set of weights satisfying a prescribed Lipschitz bound is highly non-convex, complicating training. Both (Rosca et al.) and (Dawson et al., 2023) specifically highlight the

computationally-intensive nature of these bounds as limitations for applications. We will continue to discuss related work below, but first we state the main contributions of this paper.

Contribution. In this paper we introduce a new parameterization of neural networks, both fully-connected multi-layer perceptions (MLP) and deep convolutional neural networks (CNN), which has *built-in* guarantees on the network’s Lipschitz bound, equivalent the best-known bounds provided by the SDP method (Fazlyab et al., 2019). Roughly speaking, we construct a smooth surjective mapping from an unconstrained parameter space \mathbb{R}^N onto the (non-convex) set of network weights satisfying these bounds.

This enables learning of lipschitz-bounded networks via standard unconstrained optimization methods such as stochastic gradient methods or ADAM (Kingma & Ba, 2015), avoiding the complex projection steps or barrier function computations that have previously been required and limited scalability.

Related Work. This work sits in the broader context of methods to certify safety and robustness of neural networks. This includes interval propagation bounds (see e.g. (Gowal et al., 2018)) which are simple but can be conservative, to methods based on convex relaxation (e.g. (Raghunathan et al., 2018) and (Wong & Kolter, 2018)) and mixed-integer programming (Tjeng et al., 2019).

Specific to computation of Lipschitz bounds, (Szegedy et al., 2014) already suggested analysis via layer-wise spectral bounds. (Tsuzuku et al., 2018) proposed a computationally tractable approach for convolutional models, based on layer-wise estimates of spectral norm. (Anil et al., 2019) proposed a novel activation function and associated weight constraints. (Gouk et al., 2021) presented training methods incorporating Lipschitz bounds for multiple norms, using a power iteration method to approximate spectral norms for the ℓ^2 case. (Aquino et al., 2022) bounded Lipschitz constants via incremental dissipativity theory. Beyond standard feedforward networks, (Revay et al., 2020) proposed a class of Lipschitz-bounded equilibrium networks and (Revay et al., 2021) extended this to recurrent (dynamic) equilibrium networks.

Since the SDP-based bounds of (Fazlyab et al., 2019) appeared, several papers have proposed methods to allow training of Lipschitz models. (Pauli et al., 2021), which proposed an alternating direction method of multipliers (ADMM) approach, which required solving an SDP at each iteration. (Newton & Papachristodoulou, 2021) and (Xue et al., 2022) improve computational tractability by exploiting chordal sparsity. Moving beyond the fully-connected case, (Pauli et al., 2022) proposed a method based on 2D systems theory

to certify 1D convolutional networks.

Notation. Let \mathbb{R}, \mathbb{C} be the set of real and complex numbers, respectively. Throughout the paper we have

$$\mathbb{J}_+^n := \{\text{diagonal } J \in \mathbb{R}^{n \times n} \mid J_{ii} \in [0, 1], \forall 1 \leq i \leq n\},$$

$$\mathbb{D}_{++}^n := \{\text{diagonal } D \in \mathbb{R}^{n \times n} \mid D_{ii} > 0, \forall 1 \leq i \leq n\}.$$

$A \succeq 0$ means that A is positive semi-definite. For a vector $x \in \mathbb{R}^n$, its 2-norm is denoted by $\|x\|$. Given a matrix $A \in \mathbb{R}^{m \times n}$, $\|A\|$ is defined as its the largest singular value and A^+ is its generalized inverse.

2. Problem Setup and Preliminaries

Consider an L -layer feed-forward neural network $y = f(x)$ described by the following recursive equations:

$$\begin{aligned} z_0 &= x, \\ z_{k+1} &= \sigma(W_k z_k + b_k), \quad k = 0, \dots, L-1 \\ y &= W_L z_L + b_L, \end{aligned} \quad (1)$$

where $x \in \mathbb{R}^{n_0}, z_k \in \mathbb{R}^{n_k}, y \in \mathbb{R}^{n_{L+1}}$ are the network input, hidden unit of the k th layer and network output, respectively. Here $W_k \in \mathbb{R}^{n_{k+1} \times n_k}$ and $b_k \in \mathbb{R}^{n_{k+1}}$ are the weight matrix and bias vector for the k th layer. We make the following assumption on σ , which holds for commonly-used activation functions (Goodfellow et al., 2016).

Assumption 2.1. The nonlinear activation $\sigma : \mathbb{R} \rightarrow \mathbb{R}$ is piecewise differentiable and sloped restricted in $[0, 1]$.

Note also that if different channels have different activation functions, then we simply require that they all satisfy the above assumption.

Definition 2.2. A feed-forward neural network f of the form (1) is said to be globally Lipschitz bounded by $\gamma > 0$ (or simply γ -Lipschitz) if

$$\|f(x_1) - f(x_2)\| \leq \gamma \|x_1 - x_2\|, \quad \forall x_1, x_2 \in \mathbb{R}^{n_0}. \quad (2)$$

The main goal of this work is to learn feed-forward networks (1) with certificated Lipschitz bound of γ , i.e.,

$$\min_{\theta} \mathcal{L}(f_{\theta}) \quad \text{s.t.} \quad \text{Lip}(f_{\theta}) \leq \gamma \quad (3)$$

where $\mathcal{L}(\cdot)$ is a loss function. Since it is NP-hard to compute $\text{Lip}(f_{\theta})$. We need an accurate Lipschitz bound estimation so that the constraint in (3) does not lead to a significant restriction on the model expressivity.

In (Fazlyab et al., 2019), integral quadratic constraint (IQC) theory was applied to capture both monotonicity and 1-Lipschitzness properties of σ , leading to a state-of-art tight

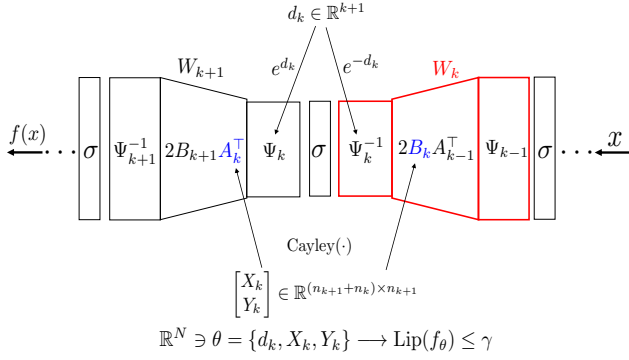


Figure 1. Direct parameterization for Lipschitz-bounded deep networks.

Lipschitz bound estimation based on the following linear matrix inequality (LMI), see details in Appendix A:

$$H := \begin{bmatrix} \gamma I & -U^\top \Lambda & 0 \\ -\Lambda U & 2\Lambda - \Lambda W - W^\top \Lambda & -Y^\top \\ 0 & -Y & \gamma I \end{bmatrix} \succeq 0 \quad (4)$$

where $\Lambda \in \mathbb{D}_{++}^n$ with $n = \sum_{k=1}^L n_k$, and

$$W = \begin{bmatrix} 0 & & & \\ W_1 & \ddots & & \\ \vdots & \ddots & 0 & \\ 0 & \cdots & W_{L-1} & 0 \end{bmatrix}, \quad U = \begin{bmatrix} W_0 \\ 0 \\ \vdots \\ 0 \end{bmatrix},$$

$$Y = \begin{bmatrix} 0 & \cdots & 0 & W_L \end{bmatrix}.$$

Although (4) can be converted into a convex constraint for Lipschitz bound estimation of a network with fixed W, U, Y , the learning problem in (3) is highly nonconvex due to changeable W, U, Y . For even relatively small-scale networks (e.g. ~ 1000 neurons), the associate barrier terms or projections become a major computational bottleneck.

Remark 2.3. The published paper (Fazlyab et al., 2019) claimed that even tighter Lipschitz bounds could be achieved with a less restrictive class of multipliers Λ than diagonal. However, this claim was false: a counterexample was presented in (Pauli et al., 2021), and an explanation of the error was presented in (Revay et al., 2020).

3. Model parameterization

In this section we will present a model parameterization (see Figure 1) such that the learning problem (3) with complicated matrix inequality constraint (4) can be transformed into an unconstrained optimization problem.

Definition 3.1. A mapping $\mathcal{M}_\Theta : \theta \in \Theta \subseteq \mathbb{R}^N \mapsto f_\theta$ is called a parameterization of DNNs with Lipschitz bound

of γ if f_θ is γ -Lipschitz for any $\theta \in \Theta$. Furthermore, such mapping is called a *direct parameterization* if $\Theta = \mathbb{R}^N$.

The free parameter θ in the proposed direct parameterization consists of

$$d_j \in \mathbb{R}^{n_{j+1}}, \quad j = 0, \dots, L-1, \\ X_k \in \mathbb{R}^{n_{k+1} \times n_{k+1}}, Y_k \in \mathbb{R}^{n_k \times n_{k+1}}, \quad k = 0, \dots, L.$$

Note that bias terms are dropped for simplicity. Based these parameters, we first construct

$$\Psi_j = \text{diag}(e^{d_j}), \quad \begin{bmatrix} A_k^\top \\ B_k^\top \end{bmatrix} = \text{Cayley} \left(\begin{bmatrix} X_k \\ Y_k \end{bmatrix} \right) \quad (5)$$

where the Cayley transform is defined as

$$\text{Cayley} \left(\begin{bmatrix} X \\ Y \end{bmatrix} \right) := \begin{bmatrix} (I + Z)^{-1}(I - Z) \\ -2Y(I + Z)^{-1} \end{bmatrix} \quad (6)$$

with $Z = X - X^\top + Y^\top Y$. Then, the weight matrices of (1) are given by

$$W_k = 2\Psi_k^{-1}B_kA_{k-1}^\top\Psi_{k-1}, \quad k = 0, \dots, L \quad (7)$$

where $A_{-1} = I, \Psi_{-1} = \sqrt{\gamma/2}I$ and $\Psi_L = \sqrt{2/\gamma}I$ with γ as the prescribed Lipschitz bound. Notice that weight k depends on parameters of index k and $k-1$, i.e. there is an “interlacing” coupling between parameters and weights.

The proposed approach is mainly based on the observation that the structure of H in (4) is a chordal graph. Thus, any semi-definite matrix with such structure can be parameterized by $H = PP^\top$ where

$$P = \begin{bmatrix} D_{-1} & & & & \\ -V_0 & D_0 & & & \\ & \ddots & \ddots & & \\ & & -V_L & D_L & \end{bmatrix}.$$

Substituting the above parameterization into (4) yields (6), see detailed derivation in Appendix B.

The main theoretical results is that our parameterization is *complete* (necessary and sufficient) for the set of DNNs satisfying the LMI constraint (4) of (Fazlyab et al., 2019).

Theorem 3.2. The forward network (1) satisfies the LMI condition (4) iff its weight matrices W_k can be parameterized via (7).

The proof of this and all other theorems can be found in the appendix.

3.1. 1-Lipschitz sandwich layer

The proposed parameterization can also be interpreted as a new layer type. By introducing new hidden units $h_k =$

$\sqrt{2}A_k^\top \Psi_k z_k$ for $k = 0, \dots, L$, we can rewrite the proposed γ -LBDN as

$$\begin{aligned} h_0 &= \sqrt{\gamma}x \\ h_{k+1} &= \sqrt{2}A_k^\top \Psi_k \sigma(\sqrt{2}\Psi_k^{-1}B_k h_k + b_k) \\ y &= \sqrt{\gamma}B_L h_L + b_L. \end{aligned} \quad (8)$$

The core component of the above model is a sandwich-structured layer of the form:

$$h_{\text{out}} = \sqrt{2}A^\top \Psi \sigma(\sqrt{2}\Psi^{-1}B h_{\text{in}} + b) \quad (9)$$

where $h_{\text{in}} \in \mathbb{R}^p, h_{\text{out}} \in \mathbb{R}^q$ are the layer input and output, respectively. Unlike the parameterization in (7), consecutive layers in (8) does not have coupled free parameters, which allows for modular implementation. Another advantage is that such representation can reveal some fundamental insights on the roles of Ψ, A and B .

Theorem 3.3. *The layer (9) with Ψ, A, B constructed by (5) is 1-Lipschitz.*

Remark 3.4. Our proposed 1-Lipschitz layer can also incorporate more structured linear operators such as *convolution*, see more details in Appendix C.

To understand the role of Ψ , we look at a simple nonlinear activation layer which is obtained simply by placing $\Psi \in \mathbb{D}_{++}^q$ and its inverse after and before σ , i.e.,

$$u = \Psi \sigma(\Psi^{-1}v + b). \quad (10)$$

Here Ψ can change the shape and shift the position of individual activation channel while keeping their slopes within $[0, 1]$, allowing the optimizer to search over a rich set of activations.

For the roles of A and B , we need to look at another special case of (9) where σ is the identity operator. Then, (9) becomes a linear layer

$$h_{\text{out}} = 2A^\top B h_{\text{in}} + \hat{b}. \quad (11)$$

As a direct corollary of Theorem 3.3, the above linear layer is 1-Lipschitz, i.e., $\|2A^\top B\| \leq 1$. We show that such parameterization is *complete* for 1-Lipschitz linear layers.

Proposition 3.5. *A linear layer is 1-Lipschitz iff its weight W satisfies $W = 2A^\top B$ with A, B given by (5).*

Comparison to existing 1-Lipschitz linear layers.

Many existing 1-Lipschitz DNNs are constructed based on 1-Lipschitz linear layers (Tsuzuku et al., 2018; Trockman & Kolter, 2021; Singla & Feizi, 2021; Singla et al., 2022; Prach & Lampert, 2022). The overall network Lipschitz bound is then obtained via spectral norm bound, i.e., $\|\text{Lip}(f)\| \leq \prod_{k=0}^L \|W_k\| \leq 1$. Our model parameterization allows for both the individual layer and network spectral bound to be larger than 1, while the network Lipschitz constant is still bounded by a weighted layerwise spectral bound of 1.

Proposition 3.6. *The DNN (7) with $\gamma = 1$ satisfies the weighted spectral norm bound $\|\tilde{W}_k\| \leq 1, 0 \leq k \leq L$, where $\tilde{W}_k = \frac{1}{2}B_k^\top \Psi_k W_k \Psi_{k-1}^{-1}(A_{k-1}^\top)^+$. Moreover, it is also 1-Lipschitz as $\text{Lip}(f) \leq \prod_{k=0}^L \|\tilde{W}_k\| \leq 1$.*

Comparison to SLL. A recent work (Araujo et al., 2023) also proposed an SDP-based Lipschitz Layer (SLL):

$$h_s(x) = x - 2FT^{-1}\sigma(F^\top x + b)$$

where T is a positive diagonal matrix satisfying $T \succeq F^\top F$. The SLL parameterization can be treated as an analytical solution to a special case (i.e. $\gamma = 1$ and $H = I$) of the following SDP condition

$$\begin{bmatrix} \gamma I - H^\top H & -H^\top G - F\Lambda \\ -G^\top H - \Lambda F^\top & 2\Lambda - \frac{1}{\gamma}G^\top G \end{bmatrix} \succeq 0, \quad (12)$$

which is used to certificate the γ -Lipschitz property of a general layer

$$h(x) = Hx + G\sigma(F^\top x + b). \quad (13)$$

Similar to the SLL approach, the proposed sandwich parameterization (9) can also be treated as an analytical solution to another special case of (12) where $H = 0$. This is because the general structure (13) with $H = 0$ can be rewritten as a standard feed-forward network (1) with $W = 0, F = U^\top$ and $Y = G$. Then, we can easily verify that (12) is equivalent to (4).

Despite the similarities between those two layers, our Lipschitz model parameterization built on the proposed sandwich layer is complete for any DNN satisfying the (structured, network-scale) SDP in (Fazlyab et al., 2019) for any Lipschitz bound γ . In (Araujo et al., 2023), only a single layer with the ResNet structure is parameterized, and they are then composed without considered cross-layer coupling. Furthermore only the case $\gamma = 1$ was considered. If a model with $\gamma > 1$ is desired, clearly one can compose 1-Lipschitz SLL layer with γ , i.e. either $\gamma h_s(x)$ or $h_s(\gamma x)$. However, such parameterization is incomplete as the example below gives a residual layer which satisfies (12), but cannot be constructed as an SLL layer in this way.

Example 3.7. Consider the following residual layer, which has a Lipschitz bound of 1.001:

$$h(x) = x + \begin{bmatrix} 1 & 0 \\ 0 & 0.001 \end{bmatrix} \sigma \left(\begin{bmatrix} 0 & 0 \\ 0 & 1 \end{bmatrix} x + b \right).$$

It can be verified that (12) is satisfied with $\gamma = 1.001$ and $\Lambda = \text{diag}(\lambda_1, \lambda_2)$ chosen such that $\lambda_1 > (\gamma - 1/2)/(\gamma^2 - \gamma)$ and $\lambda_2 = \gamma^2 - \gamma$. However, it cannot be written as $\gamma h_s(x)$ or $h_s(\gamma x)$ since there does not exist a positive diagonal matrix T such that $G = -2FT^{-1}$.

Table 1. The table presents the tightness of Lipschitz bound of several concurrent parameterization and our approach on a toy example. The bound tightness is measured by $\underline{\gamma}/\gamma$ (%), where $\underline{\gamma}$ and γ are the empirical lower bound and certified upper bound.

MODELS	LIP. TIGHTNESS (γ)		
	1	5	10
AOL	79.3	45.1	49.2
ORTHOGONAL	73.7	72.6	61.5
SLL	99.9	90.6	68.6
SANDWICH	99.9	99.4	94.8

4. Experiments

Our experiments have two goals: First, to show that our model parameterization can provide a tight Lipschitz bounds, which we illustrate with simple curve-fitting tasks. Second, to examine the performance and scalability of the proposed new layer parameterization on adversarially robustness image classification tasks, illustrated with the CIFAR-10/100 and Tiny Imagenet datasets. Model architectures and training details can be found in the appendix.

Tightness of Lipschitz Bounds. We illustrate the tight Lipschitz bound of our model parameterization using a toy example of curve fitting:

$$\text{square wave: } f(x) = \begin{cases} 0, & x \in [-1, 0) \cup [1, 2], \\ 1, & x \in [-2, -1) \cup [0, 1). \end{cases}$$

Note that the true function has no global Lipschitz bound due to the points of discontinuity. Thus a function approximator will naturally try to find models with large local Lipschitz constant near those singular points, and if a global γ -Lipschitz constraint is imposed this is a useful test of its accuracy. We evaluate the tightness of Lipschitz bound using $\underline{\gamma}/\gamma$ where $\underline{\gamma}$ is an empirical lower Lipschitz bound obtained by a PGD-like method and γ is the imposed upper bound, which was 1, 5, and 10 in the cases we tested. In Table 1 it can be seen that our approach achieves a much tighter Lipschitz bounds compared to AOL and orthogonal layers. The SLL model has similar level of tightness when γ is small but its bound becomes more loose as γ increases compared to our model, e.g. 68.6% v.s. 94.8% for $\gamma = 10$.

In Figure 2 we break down the Lipschitz bounds and spectral norms over layers. It can be seen that all individual layers have quite tight Lipschitz bounds on a per-layer basis of around 99%. However, for the complete network the sandwich layer achieves a much tighter bound of 99.9% vs 73.7% (orthogonal) and 79.3% (AOL). This illustrates the benefits of taking into account coupling between neighborhood layers, thus allowing individual layers to have spectral norm greater than 1. We note that, for the sandwich model,

the layer-wise product of spectral norms reaches 75.8, illustrating how poor this commonly-used bound is compared to our bound.

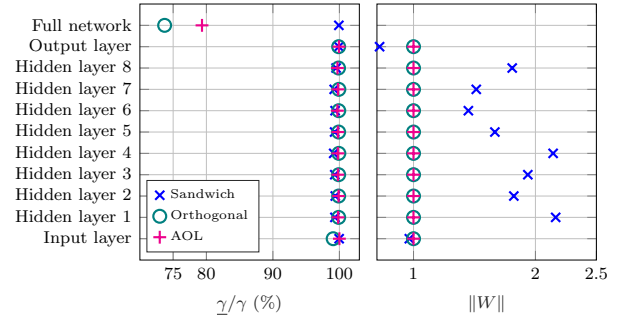


Figure 2. empirical Lipschitz bound for curve fitting of a square wave. The lower bound $\underline{\gamma}$ is obtained using PGD-like method. We observed tight layer Lipschitz bound for AOL, orthogonal and sandwich layers ($\geq 99.1\%$). However, the propose sandwich layer has a much tighter Lipschitz bound for the entire network. **Right:** the spectral norm of weight matrices. Our approach admits weight matrices with spectral norm larger than 1. The layerwise product $\prod_{k=0}^L \|W_k\|$ is about 75.8, which is much larger than that of AOL and orthogonal layers.

Adversarial Robust Training of Image Classifiers. The first case we considered was the MNIST data set with fully-connected layers. In Figure 3 we observe that the sandwich layer had lower test error than the orthogonal layer in all cases, illustrating the improved flexibility. Both layers achieved have similarly tight Lipschitz bounds, however they were not nearly as tight as in the curve fitting case. We note that with $\gamma = 0.1$ both models offer significant robustness advantages to adversarial perturbations, while Sandwich offers better nominal test error that MLP, but orthogonal layer degrades test error. In fact, the sandwich layer with $\gamma = 0.1$ achieves similar test error to the orthogonal layer $\gamma = 0.5$ and 1, while offering much better robustness.

For CIFAR10 we fit multi-layer convolutional models, and see similar trends. Again we see that Lipschitz bounds improve test error compared to a vanilla CNN, while also improving robustness dramatically. And again, the sandwich layer with $\gamma = 1$ achieves similar test error to the orthogonal layer with $\gamma = 10$, while offering much better robustness.

In Figure 4 we plot the training curves (test-error vs epoch) for the sandwich, orthogonal, and MLP/CNN models for MNIST (fully-connected models) and CIFAR-10 (convolutional models). We observe that in both cases the sandwich model surpasses the final error of the MLP/CNN in less than half as many epochs. In fact, for the fully connected case it does so in around a third as many epochs. An inter-

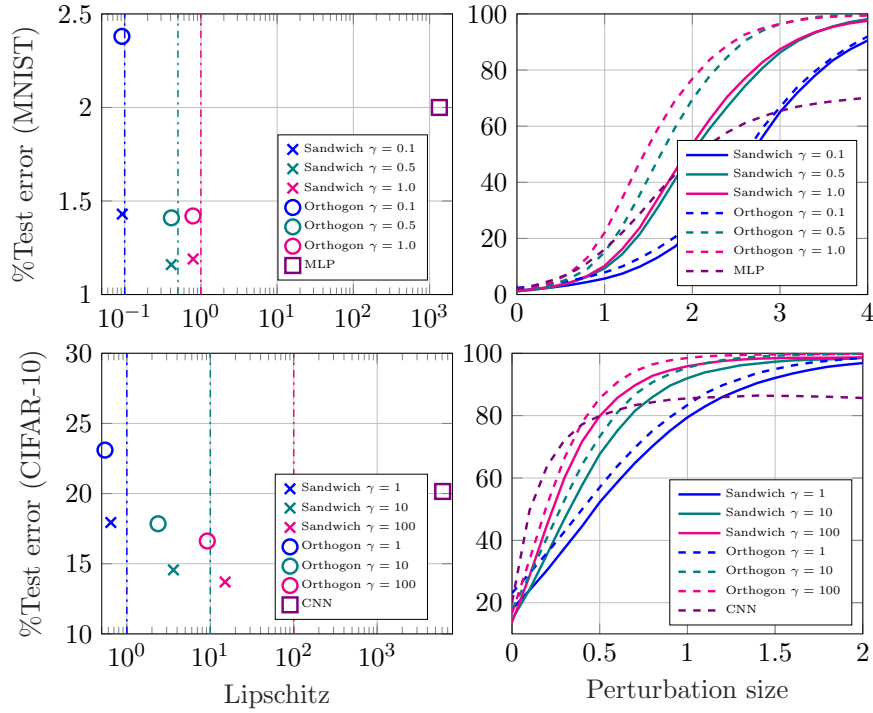


Figure 3. Image classification: test error vs Lipschitz constants (left) and robustness to adversarial perturbations (right), for MNIST with fully-connected layers (top) and CIFAR-10 with convolutional layers (bottom). Note that the proposed sandwich layer achieves both better test error and greater robustness than alternatives. The empirical robustness is measured with L2FastGradientAttack method (Rauber et al., 2017).

esting observation from Figure 4 is that both the MLP and CNN models seem to exhibit the epoch-wide double descent phenomenon (see, e.g., (Nakkiran et al., 2021a)), whereas neither of the Lipschitz bounded models (sandwich and orthogonal) do, they simply improve test error monotonically with epochs. Weight regularization has been suggested as a mitigating factor for other forms of double descent (Nakkiran et al., 2021b), however we are not aware of this specific phenomenon having been observed before.

Empirical Robustness Results on CIFAR-100 and Tiny-Imagenet. We ran further empirical tests on larger datasets such as CIFAR-100 and Tiny-Imagenet, comparing our Sandwich layer to similar approaches such as AOL, orthogonal and SLL layers. We use the same architecture in (Trockman & Kolter, 2021) for AOL, orthogonal and sandwich models with *small*, *medium* and *large* sizes. Since SLL is a residual layer, we use the architecture proposed by (Araujo et al., 2023) whose model size are much larger than those non-residual networks. In this setup we trained models with Lipschitz bounds of $\{0.5, 1, 2, \dots, 16\}$ and presented the one with best robust accuracy for $\epsilon = 36/255$. The results along with total number of parameters (NP) and training time per epoch (TpE) are collected in Table 2.

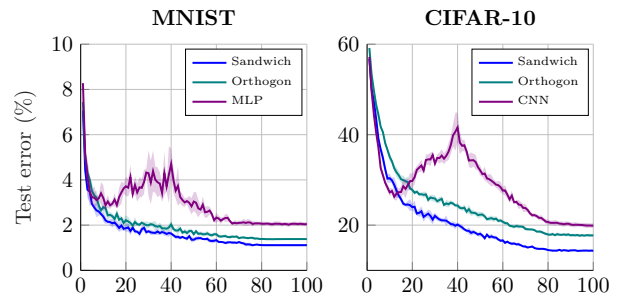


Figure 4. Learning curves and training time per epoch for image classification tasks, obtained from 5 experiments. The Lipschitz bounds are 0.5 for MNIST and 10 for CIFAR-10. Note that the “double-descent” phenomenon is avoided with the Lipschitz-bounded models.

Table 2. This table presents the clean, empirical robust accuracy as well as the number of parameters and training time of several concurrent work and our sandwich model on CIFAR-100 and Tiny-ImageNet datasets. Input data is normalized and no last layer normalization is implemented. The Lipschitz bounds for CIFAR-100 and Tiny-ImageNet are 2 and 1, respectively. The empirical robustness is measured with *AutoAttack* (Croce & Hein, 2020).

DATASETS	MODELS	CLEAN ACC.	AUTOATTACK (ϵ)			NUMBER OF PARAMETERS	TIME BY EPOCH
			$\frac{36}{255}$	$\frac{72}{255}$	$\frac{108}{255}$		
CIFAR100	ORTHOGON SMALL	48.2	38.7	30.5	24.1	3M	17s
	ORTHOGON MEDIUM	51.2	40.9	32.5	25.8	12M	20s
	ORTHOGON LARGE	51.8	42.5	34.1	27.6	48M	55s
	AOL SMALL	31.8	25.8	21.2	17.2	3M	16s
	AOL MEDIUM	32.8	26.8	22.5	18.4	12M	17s
	AOL LARGE	33.6	28.1	23.5	19.2	48M	29s
	SLL SMALL	53.1	42.2	33.1	25.6	41M	26s
	SLL MEDIUM	53.8	43.1	33.9	26.5	78M	48s
	SLL LARGE	55.2	44.3	34.7	27.3	118M	109s
	SANDWICH SMALL	54.4	44.5	35.4	28.3	3M	18s
	SANDWICH MEDIUM	56.0	46.6	37.9	31.1	12M	21s
	SANDWICH LARGE	57.4	48.3	40.0	32.8	48M	78s
TINYIMAGENET	ORTHOGON SMALL	29.5	24.6	19.9	16.2	10M	57s
	ORTHOGON MEDIUM	31.3	25.9	21.3	17.5	44M	90s
	AOL SMALL	16.5	14.0	12.0	10.1	10M	54s
	AOL MEDIUM	19.2	16.3	14.2	12.0	44M	67s
	SLL SMALL	29.3	23.8	18.5	14.5	165M	198s
	SLL MEDIUM	30.8	24.8	19.6	15.7	315M	450s
	SANDWICH SMALL	35.3	29.6	24.9	20.6	10M	68s
	SANDWICH MEDIUM	35.2	30.0	25.5	21.6	37M	138s

Since data are normalized before feeding to the models, the effective Lipschitz bounds are roughly 4 times larger.

We observe that our proposed Sandwich layer achieves uniformly the best results (around 5% improvement) over those two data sets, all model sizes, and both clean accuracy and robust accuracy with all perturbation sizes. Furthermore, our Sandwich model can achieve superior results with much smaller models and faster training. On CIFAR-100, comparing our Sandwich-medium vs SLL-large we see that ours gives superior clean and robust accuracy despite having only 12M parameters vs 118M, and taking only 21s vs 109s TpE. Similarly on Tiny-Imagenet: comparing our Sandwich-small vs SLL-medium, ours has much better clean and robust accuracy, despite having 10M parameters vs 315M, and taking 68s vs 450s TpE.

Results on Certified Robustness. We also compare the certified robustness to the SLL approach which outperforms most existing 1-Lipschitz networks (Araujo et al., 2023). Slightly different from the previous experimental setup for empirical robustness comparison, we remove the data normalization and use the Last Layer Normalization (LLN) proposed by (Singla et al., 2022) which improves the certified accuracy when the number of classes becomes large. Due to LLN, the composited model is not 1-Lipschitz during training. The certified accuracy is then normalized by

the last layer, see more details in (Singla et al., 2022).

From Table 3 we can see that on CIFAR-100, our Sandwich model performs similarly to somewhat larger SLL models (41M parameters vs 26M, i.e. 60% increase). However it is outperformed by much larger SLL models (236M parameters, 9 times larger). With Tiny-Imagenet, we see that our uniformly outperforms SLL models, even the extra large SLL model (28 times as many parameters). Furthermore, our advantage over similarly-sized SLL models is very significant (e.g. 24.7% vs 19.5% certified accuracy for $\epsilon = 36/255$).

5. Conclusions and Future Work

In this paper we have introduced a new parameterization of neural networks that automatically satisfy the tightest currently-known computationally-tractable Lipschitz bounds. This enables learning of Lipschitz-bounded networks with standard first-order gradient methods, avoiding the need for complex projections or barrier evaluations. We have illustrated the approach on simple curve-fitting tasks and adversarially-robust image classification with both fully-connected and convolutional networks. Our future work will include exploring applications in other settings including robust reinforcement learning and control.

Table 3. This table presents the certified robust of SLL and sandwich model on CIFAR-100 and Tiny-ImageNet datasets. Input data is not normalized while last layer normalization is applied. Results of SLL model are from (Araujo et al., 2023).

DATASETS	MODELS	CLEAN ACC.	CERTIFIED ACC. (ϵ)			NUMBER OF PARAMETERS
			$\frac{36}{255}$	$\frac{72}{255}$	$\frac{108}{255}$	
CIFAR100	SLL SMALL	44.9	34.7	26.8	20.9	41M
	SLL XLARGE	46.5	36.5	28.4	22.7	236M
	SANDWICH	46.4	35.0	26.8	20.8	26M
TINYIMAGENET	SLL SMALL	26.6	19.5	12.2	10.4	167M
	SLL X-LARGE	32.1	23.0	16.9	12.3	1.1B
	SANDWICH	33.2	24.7	18.0	13.2	39M

References

- Anil, C., Lucas, J., and Grosse, R. Sorting out lipschitz function approximation. In *International Conference on Machine Learning*, pp. 291–301. PMLR, 2019.
- Aquino, B., Rahnama, A., Seiler, P., Lin, L., and Gupta, V. Robustness against adversarial attacks in neural networks using incremental dissipativity. *IEEE Control Systems Letters*, 6:2341–2346, 2022.
- Araujo, A., Havens, A., Delattre, B., Allauzen, A., and Hu, B. A unified algebraic perspective on lipschitz neural networks. *arXiv preprint arXiv:2303.03169*, 2023.
- Arjovsky, M., Chintala, S., and Bottou, L. Wasserstein generative adversarial networks. In *International conference on machine learning*, pp. 214–223. PMLR, 2017.
- Bartlett, P. L., Foster, D. J., and Telgarsky, M. J. Spectrally-normalized margin bounds for neural networks. In *Advances in Neural Information Processing Systems*, pp. 6240–6249, 2017.
- Brunke, L., Greeff, M., Hall, A. W., Yuan, Z., Zhou, S., Panerati, J., and Schoellig, A. P. Safe learning in robotics: From learning-based control to safe reinforcement learning. *Annual Review of Control, Robotics, and Autonomous Systems*, 5:411–444, 2022.
- Chu, Y.-C. and Glover, K. Bounds of the induced norm and model reduction errors for systems with repeated scalar nonlinearities. *IEEE Transactions on Automatic Control*, 44(3):471–483, 1999.
- Coleman, C., Narayanan, D., Kang, D., Zhao, T., Zhang, J., Nardi, L., Bailis, P., Olukotun, K., Ré, C., and Zaharia, M. Dawnbench: An end-to-end deep learning benchmark and competition. *Training*, 100(101):102, 2017.
- Croce, F. and Hein, M. Reliable evaluation of adversarial robustness with an ensemble of diverse parameter-free attacks. In *International conference on machine learning*, pp. 2206–2216. PMLR, 2020.
- D’Amato, F. J., Rotea, M. A., Megretski, A., and Jönsson, U. New results for analysis of systems with repeated nonlinearities. *Automatica*, 37(5):739–747, 2001.
- Dawson, C., Gao, S., and Fan, C. Safe control with learned certificates: A survey of neural lyapunov, barrier, and contraction methods for robotics and control. *IEEE Transactions on Robotics*, 2023.
- Fazlyab, M., Robey, A., Hassani, H., Morari, M., and Pappas, G. Efficient and accurate estimation of lipschitz constants for deep neural networks. In *Advances in Neural Information Processing Systems*, pp. 11427–11438, 2019.
- Goodfellow, I., Bengio, Y., and Courville, A. *Deep learning*. MIT press, 2016.
- Gouk, H., Frank, E., Pfahringer, B., and Cree, M. J. Regularisation of neural networks by enforcing lipschitz continuity. *Machine Learning*, 110:393–416, 2021.
- Gowal, S., Dvijotham, K., Stanforth, R., Bunel, R., Qin, C., Uesato, J., Andjelovic, R., Mann, T., and Kohli, P. On the effectiveness of interval bound propagation for training verifiably robust models. *arXiv preprint arXiv:1810.12715*, 2018.
- Gulrajani, I., Ahmed, F., Arjovsky, M., Dumoulin, V., and Courville, A. C. Improved training of wasserstein gans. *Advances in neural information processing systems*, 30, 2017.
- Jain, A. K. *Fundamentals of digital image processing*. Prentice-Hall, Inc., 1989.
- Kingma, D. P. and Ba, J. Adam: A method for stochastic optimization. *arXiv preprint arXiv:1412.6980*, 2014.
- Kingma, D. P. and Ba, J. L. Adam: A method for stochastic gradient descent. In *ICLR: International Conference on Learning Representations*, 2015.

- Kulkarni, V. V. and Safonov, M. G. All multipliers for repeated monotone nonlinearities. *IEEE Transactions on Automatic Control*, 47(7):1209–1212, 2002.
- Li, Q., Haque, S., Anil, C., Lucas, J., Grosse, R. B., and Jacobsen, J.-H. Preventing gradient attenuation in lipschitz constrained convolutional networks. *Advances in neural information processing systems*, 32, 2019.
- Liu, H.-T. D., Williams, F., Jacobson, A., Fidler, S., and Litany, O. Learning smooth neural functions via lipschitz regularization. In *ACM SIGGRAPH 2022 Conference Proceedings*, pp. 1–13, 2022.
- Madry, A., Makelov, A., Schmidt, L., Tsipras, D., and Vladu, A. Towards deep learning models resistant to adversarial attacks. In *International Conference on Learning Representations*, 2018.
- Nakkiran, P., Kaplun, G., Bansal, Y., Yang, T., Barak, B., and Sutskever, I. Deep double descent: Where bigger models and more data hurt. *Journal of Statistical Mechanics: Theory and Experiment*, 2021(12):124003, 2021a.
- Nakkiran, P., Venkat, P., Kakade, S. M., and Ma, T. Optimal regularization can mitigate double descent. In *International Conference on Learning Representations*, 2021b.
- Newton, M. and Papachristodoulou, A. Exploiting sparsity for neural network verification. In *Learning for Dynamics and Control*, pp. 715–727. PMLR, 2021.
- Pauli, P., Koch, A., Berberich, J., Kohler, P., and Allgöwer, F. Training robust neural networks using lipschitz bounds. *IEEE Control Systems Letters*, 6:121–126, 2021.
- Pauli, P., Gramlich, D., and Allgöwer, F. Lipschitz constant estimation for 1d convolutional neural networks. *arXiv preprint arXiv:2211.15253*, 2022.
- Prach, B. and Lampert, C. H. Almost-orthogonal layers for efficient general-purpose lipschitz networks. In *Computer Vision–ECCV 2022: 17th European Conference, Tel Aviv, Israel, October 23–27, 2022, Proceedings, Part XXI*, pp. 350–365. Springer, 2022.
- Raghunathan, A., Steinhardt, J., and Liang, P. Certified Defenses against Adversarial Examples. In *International Conference on Learning Representations*, 2018.
- Rauber, J., Brendel, W., and Bethge, M. Foolbox: A python toolbox to benchmark the robustness of machine learning models. *arXiv preprint arXiv:1707.04131*, 2017.
- Revay, M., Wang, R., and Manchester, I. R. Lipschitz bounded equilibrium networks. *arXiv:2010.01732*, 2020.
- Revay, M., Wang, R., and Manchester, I. R. Recurrent equilibrium networks: Unconstrained learning of stable and robust dynamical models. In *2021 60th IEEE Conference on Decision and Control (CDC)*, pp. 2282–2287. IEEE, 2021.
- Rosca, M., Weber, T., Gretton, A., and Mohamed, S. A case for new neural networks smoothness constraints. In *“I Can’t Believe It’s Not Better!” NeurIPS 2020 workshop*.
- Russo, A. and Proutiere, A. Towards optimal attacks on reinforcement learning policies. In *2021 American Control Conference (ACC)*, pp. 4561–4567. IEEE, 2021.
- Singla, S. and Feizi, S. Skew orthogonal convolutions. In *International Conference on Machine Learning*, pp. 9756–9766. PMLR, 2021.
- Singla, S., Singla, S., and Feizi, S. Improved deterministic l2 robustness on cifar-10 and cifar-100. In *International Conference on Learning Representations*, 2022.
- Szegedy, C., Zaremba, W., Sutskever, I., Bruna, J., Erhan, D., Goodfellow, I., and Fergus, R. Intriguing properties of neural networks. In *ICLR: International Conference on Learning Representations*, 2014.
- Tjeng, V., Xiao, K. Y., and Tedrake, R. Evaluating robustness of neural networks with mixed integer programming. In *International Conference on Learning Representations*, 2019.
- Trockman, A. and Kolter, J. Z. Orthogonalizing convolutional layers with the cayley transform. *arXiv preprint arXiv:2104.07167*, 2021.
- Tsuzuku, Y., Sato, I., and Sugiyama, M. Lipschitz-margin training: Scalable certification of perturbation invariance for deep neural networks. In *Advances in neural information processing systems*, pp. 6541–6550, 2018.
- Virmaux, A. and Scaman, K. Lipschitz regularity of deep neural networks: analysis and efficient estimation. *Advances in Neural Information Processing Systems*, 31, 2018.
- Wang, R. and Manchester, I. R. Youla-ren: Learning nonlinear feedback policies with robust stability guarantees. In *2022 American Control Conference (ACC)*, pp. 2116–2123, 2022.
- Winston, E. and Kolter, J. Z. Monotone operator equilibrium networks. *Advances in neural information processing systems*, 33:10718–10728, 2020.
- Wong, E. and Kolter, Z. Provable defenses against adversarial examples via the convex outer adversarial polytope. In *International conference on machine learning*, pp. 5286–5295. PMLR, 2018.

Xue, A., Lindemann, L., Robey, A., Hassani, H., Pappas, G. J., and Alur, R. Chordal sparsity for lipschitz constant estimation of deep neural networks. In *2022 IEEE 61st Conference on Decision and Control (CDC)*, pp. 3389–3396. IEEE, 2022.

Zheng, Y., Fantuzzi, G., and Papachristodoulou, A. Chordal and factor-width decompositions for scalable semidefinite and polynomial optimization. *Annual Reviews in Control*, 52:243–279, 2021.

A. Preliminaries on LMI-based Lipschitz bound estimation

Here we review the theoretical work of LMI-based Lipschitz bound estimation for neural networks from (Fazlyab et al., 2019; Revay et al., 2020). Consider an L -layer forward network $y = f(x)$ described by the following recursive equation:

$$\begin{aligned} z_0 &= x, \\ z_{k+1} &= \sigma(W_k z_k + b_k), \quad k = 0, \dots, L-1, \\ y &= W_L z_L + b_L, \end{aligned} \quad (14)$$

where $x \in \mathbb{R}^{n_0}$, $z_k \in \mathbb{R}^{n_k}$, $y \in \mathbb{R}^{n_{L+1}}$ are the network input, hidden unit of the k th layer and network output, respectively. We stack all hidden unit z_1, \dots, z_L together and obtain a compact form of (14) as follows:

$$\begin{aligned} \begin{bmatrix} z_1 \\ z_2 \\ \vdots \\ z_L \end{bmatrix} &= \sigma \left(\overbrace{\begin{bmatrix} 0 & & & \\ W_1 & \ddots & & \\ \vdots & \ddots & 0 & \\ 0 & \dots & W_{L-1} & 0 \end{bmatrix}}^W \begin{bmatrix} z_1 \\ z_2 \\ \vdots \\ z_L \end{bmatrix} + \overbrace{\begin{bmatrix} W_0 \\ 0 \\ \vdots \\ 0 \end{bmatrix}}^U x + \overbrace{\begin{bmatrix} b_0 \\ b_1 \\ \vdots \\ b_{L-1} \end{bmatrix}}^{b_z} \right), \\ y &= \overbrace{\begin{bmatrix} 0 & \dots & 0 & W_L \end{bmatrix}}^Y \begin{bmatrix} z_1 \\ z_2 \\ \vdots \\ z_L \end{bmatrix} + \overbrace{b_L}^{b_y}. \end{aligned} \quad (15)$$

By introducing an intermediate variable $v \in \mathbb{R}^n$ with $n = \sum_{k=1}^L n_k$, we can rewrite the above equation by

$$v = Wz + Ux + b_z, \quad z = \sigma(v), \quad y = Yz + b_y. \quad (16)$$

Given two different solutions $s^a = (x^a, v^a, z^a, y^a)$ and $s^b = (x^b, v^b, z^b, y^b)$, their difference $\Delta s = s^b - s^a$ satisfies

$$\Delta v = W\Delta z + U\Delta x, \quad \Delta z = \sigma(v^b) - \sigma(v^a) := J^{ab}\Delta v, \quad \Delta y = Y\Delta z \quad (17)$$

where $J^{ab} \in \mathbb{J}_+^q$. For any Lipschitz bound $\gamma > 0$ we have $\gamma^2 \|\Delta x\|^2 - \|\Delta y\|^2 \geq 0$ holds for all nonzero Δs satisfying (17). The main challenge is how to handle the varying weight J^{ab} . One way is to replace it with a quadratic inequality constraint, which might be conserve but easy to analyze.

Lemma A.1. *If Assumption 2.1 holds, then for any $\Lambda \in \mathbb{D}_{++}^n$ the following incremental quadratic constraint (iQC) holds for any pair of (v^a, z^a) and (v^b, z^b) satisfying $z = \sigma(v)$:*

$$\begin{bmatrix} \Delta v^\top \\ \Delta z^\top \end{bmatrix}^\top \begin{bmatrix} 0 & \Lambda \\ \Lambda & -2\Lambda \end{bmatrix} \begin{bmatrix} \Delta v \\ \Delta z \end{bmatrix} \geq 0 \quad (18)$$

where $\Delta v = v^b - v^a$ and $\Delta z = z^b - z^a$.

Remark A.2. Assumption 2.1 implies that each channel satisfies $2\Delta z_i(\Delta v_i - \Delta z_i) \geq 0$, which can be leads to (18) by a linear conic combination of each channel with multiplier $\Lambda \in \mathbb{D}_{++}^n$. In (Fazlyab et al., 2019) it was claimed that iQC (18) holds with a richer (more powerful) class of multipliers (i.e. Λ is a symmetric matrix), which were previously introduced for robust stability analysis of systems with repeated nonlinearities (Chu & Glover, 1999; D'Amato et al., 2001; Kulkarni & Safonov, 2002). However this is not true: a counterexample was given in (Pauli et al., 2021), and here we give a brief explanation: even if the nonlinearities $\sigma(v_i)$ are repeated when considered as functions of v_i , their increments $\Delta z_i = \sigma(v_i^a + \Delta v_i) - \sigma(v_i^a)$ are not repeated when considered as functions of Δv_i , since the diagonal elements of J^{ab} depend on the particular v_i^a which generally differs between units.

Theorem A.3. *The feedforward neural network (14) is γ -Lipschitz if Assumption 2.1 holds, and there exist an $\Lambda \in \mathbb{D}_{++}^n$ satisfying the following LMI:*

$$H := \begin{bmatrix} \gamma I & -U^\top \Lambda & 0 \\ -\Lambda U & 2\Lambda - \Lambda W - W^\top \Lambda & -Y^\top \\ 0 & -Y & \gamma I \end{bmatrix} \succeq 0. \quad (19)$$

Remark A.4. In (Revay et al., 2020), the above LMI condition also applies to more general network structures with full weight matrix W . An equivalent form of (19) was applied in (Fazlyab et al., 2019) for a tight Lipschitz bound estimation:

$$\min_{\gamma, \Lambda} \gamma \quad \text{s.t.} \quad (19) \quad (20)$$

which can be solved by convex programming for moderate models, e.g., $n < 10K$ in (Fazlyab et al., 2019).

B. Derivation of direct parameterization

First, by substituting W, U, Y and Λ into (19), its left-hand side can be rewritten as

$$H = \begin{bmatrix} \gamma I & -W_0^\top \Lambda_0 & & & & \\ -\Lambda_0 W_0 & 2\Lambda_0 & -W_1^\top \Lambda_1 & & & \\ & -\Lambda_1 W_1 & 2\Lambda_1 & \ddots & & \\ & & \ddots & \ddots & \ddots & \\ & & & \ddots & 2\Lambda_{L-2} & -W_{L-1}^\top \Lambda_{L-1} \\ & & & & -\Lambda_{L-1} W_{L-1} & 2\Lambda_{L-1} & -W_L^\top \\ & & & & & -W_L & \gamma I \end{bmatrix}. \quad (21)$$

Note that $H \succeq 0$ has a chordal structure, which means that it can be factorized as $H = PP^\top$ with

$$P = \begin{bmatrix} D_{-1} & & & & \\ -V_0 & D_0 & & & \\ & \ddots & \ddots & & \\ & & -V_L & D_L & \end{bmatrix}.$$

By substituting it back into (21) we have

$$D_{-1}D_{-1}^\top = \gamma I, \quad V_k V_k^\top + D_k D_k^\top = 2\Lambda_k, \quad 0 \leq k < L, \quad V_L V_L^\top + D_L D_L^\top = \gamma I, \quad (22)$$

$$W_k = \Lambda_k^{-1} V_k D_{k-1}^\top. \quad (23)$$

By defining $\Psi_k = \Lambda_k^{\frac{1}{2}}$, $A_k := \sqrt{2}\Psi_k D_k$ and $B_k := \sqrt{2}\Psi_k V_k^\top$ with $k = 0, \dots, L-1$ we have $A_k A_k^\top + B_k B_k^\top = I$. Then, we can easily parameterize (Ψ_k, A_k, B_k) via simple exponential mapping of diagonal matrices and Cayley transformation on full matrices, see (6). Finally, we can obtain the weight matrices as follows

$$W_k = \Lambda_k^{-1} V_k D_{k-1}^\top = \Psi_k^{-2} \times (\sqrt{2}\Psi_k B_k) \times (\sqrt{2}A_{k-1}^\top \Psi_{k-1}) = 2\Psi_k^{-1} B_k A_{k-1}^\top \Psi_{k-1} \quad (24)$$

with $k = 0, \dots, L-1$, where $A_{-1} = I$ and $\Psi_{-1} = \sqrt{\gamma/2}I$. The above formula can also be applied to $k = L$ by choosing $\Psi_L = \sqrt{2/\gamma}I$.

C. 1-Lipschitz convolutional layer

Our proposed layer parameterization can also incorporate more structured linear operators such as convolution. Let $h_{\text{in}} \in \mathbb{R}^{p \times s \times s}$ be a p -channel image tensor with $s \times s$ spatial domain and $h_{\text{out}} \in \mathbb{R}^{q \times s \times s}$ be q -channel output tensor. We also let $A \in \mathbb{R}^{q \times q \times s \times s}$ denote a multi-channel convolution operator and similarly for $B \in \mathbb{R}^{q \times p \times s \times s}$. For the sake of simplicity, we assume that the convolutional operators A, B are circular and unstrided. Such assumption can be easily related to plain and/or 2-strided convolutions, see (Trockman & Kolter, 2021). Similar to (9), the proposed convolutional layer can be rewritten as

$$\text{Vec}(h_{\text{out}}) = \sqrt{2}\mathcal{C}_A^\top \Psi_s \sigma(\sqrt{2}\Psi_s^{-1} \mathcal{C}_B \text{Vec}(h_{\text{in}}) + b) \quad (25)$$

where $\mathcal{C}_A \in \mathbb{R}^{qs^2 \times qs^2}$, $\mathcal{C}_B \in \mathbb{R}^{qs^2 \times ps^2}$ are the doubly-circular matrix representations of A and B , respectively. For instance, $\text{Vec}(B * h_{\text{in}}) = \mathcal{C}_B \text{Vec}(h_{\text{in}})$ where $*$ is the convolution operator. We choose $\Psi_s = \Psi \otimes I_s$ with $\Psi = \text{diag}(e^d)$ so that individual channel has a constant scaling factor. To ensure that (25) is 1-Lipschitz, we need to construct $\mathcal{C}_A, \mathcal{C}_B$ using the Cayley transformation (6), which involves inverting a highly-structured large matrix $I + \mathcal{C}_Z \in \mathbb{R}^{qs^2 \times qs^2}$.

Algorithm 1 1-Lipschitz convolutional layer**Require:** $h_{\text{in}} \in \mathbb{R}^{p \times s \times s}$, $P \in \mathbb{R}^{(p+q) \times q \times s \times s}$, $d \in \mathbb{R}^q$

- 1: $\tilde{h}_{\text{in}} \leftarrow \text{FFT}(h_{\text{in}})$
- 2: $\Psi \leftarrow \text{diag}(e^d)$, $[\tilde{A} \ \tilde{B}]^* \leftarrow \text{Cayley}(\text{FFT}(P))$
- 3: $\tilde{h}[:, i, j] \leftarrow \sqrt{2}\Psi^{-1}\tilde{B}[:, :, i, j]\tilde{h}_{\text{in}}[:, i, j]$
- 4: $\tilde{h} \leftarrow \text{FFT}(\sigma(\text{FFT}^{-1}(\tilde{h}) + b))$
- 5: $\tilde{h}_{\text{out}}[:, i, j] \leftarrow \sqrt{2}A[:, :, i, j]^*\Psi\tilde{h}[:, i, j]$
- 6: $h_{\text{out}} \leftarrow \text{FFT}^{-1}(\tilde{h}_{\text{out}})$

Thanks to the doubly-circular structure, we can perform efficient computation on the Fourier domain. Taking a 2D case for example, circular convolution of two matrices is simply the elementwise product of their representations in the Fourier domain (Jain, 1989). In (Trockman & Kolter, 2021), the 2D convolution theorem was extended to multi-channel circular convolutions of tensors, which are reduced to a batch of complex matrix-vector products in the Fourier domain rather than elementwise products. For example, the Fourier-domain output related to the $(i, j)^{\text{th}}$ pixel is a matrix-vector product:

$$\text{FFT}(B * h_{\text{in}})[:, i, j] = \tilde{B}[:, :, i, j]\tilde{h}_{\text{in}}[:, i, j].$$

where $\tilde{B}[:, :, i, j] \in \mathbb{C}^{q \times p}$ and $\tilde{h}_{\text{in}}[:, i, j] \in \mathbb{C}^p$. Here $\tilde{x} = \text{FFT}(x)$ is the fast Fourier transformation (FFT) of a multi-channel tensor $x \in \mathbb{R}^{c_1 \times \dots \times c_r \times s \times s}$:

$$\text{FFT}(x)[i_1, \dots, i_r, :, :] = \mathcal{F}_s x[i_1, \dots, i_r, :, :] \mathcal{F}_s^*$$

where $\mathcal{F}_s[i, j] = \frac{1}{s} e^{-2\pi i(i-1)(j-1)\iota/s}$ with $\iota = \sqrt{-1}$. Moreover, transposing or inverting a convolution is equivalent to applying the complex version of the same operation to its Fourier domain representation – a batch of small complex matrices:

$$\begin{aligned} \text{FFT}(A^\top)[:, :, i, j] &= \tilde{A}[:, :, i, j]^*, \\ \text{FFT}((I + Z)^{-1})[:, :, i, j] &= (I + \tilde{Z}[:, :, i, j])^{-1}. \end{aligned}$$

Since the FFT of a real tensor is Hermitian-symmetric, the batch size can be reduced to $s \times (\lfloor s/2 \rfloor + 1)$.

We now give both model parameterization and forward computation of a 1-Lipschitz convolutional layer in Algorithm 1. In line 1 and 6, we use the (inverse) FFT on the input/output tensor, which can be either/both removed for multiple consecutive convolutional layers. In line 2, we perform the Cayley transformation of convolutions in the Fourier domain, which involves $s \times (\lfloor s/2 \rfloor + 1)$ parallel complex matrix inverse of size $q \times q$. In line 3-5, all operations related to the $(i, j)^{\text{th}}$ term can be done in parallel.

D. Proofs

D.1. Proof of Lemma A.1

By substituting $\Delta z = J^{ab} \Delta v$ into (18) we have

$$\begin{bmatrix} \Delta v^\top \\ \Delta z^\top \end{bmatrix}^\top \begin{bmatrix} 0 & \Lambda \\ \Lambda & -2\Lambda \end{bmatrix} \begin{bmatrix} \Delta v \\ \Delta z \end{bmatrix} = 2\Delta z^\top \Lambda (\Delta v - \Delta z) = 2\Delta v^\top J^{ab} \Lambda (I - J^{ab}) \Delta v \geq 0$$

where the last inequality follows as $J^{ab} \in \mathbb{J}_+^q$.

D.2. Proof of Theorem A.3

We first apply Schur complement to (19), which yields

$$\begin{bmatrix} \gamma I & -U^\top \Lambda \\ -\Lambda U & 2\Lambda - \Lambda W - W^\top \Lambda - \frac{1}{\gamma} Y^\top Y \end{bmatrix} \succ 0.$$

Then, by left-multiplying the above equation by $[\Delta x^\top \ \Delta z^\top]$ and right-multiplying $[\Delta x^\top \ \Delta z^\top]^\top$ we can obtain

$$\gamma \|\Delta x\|^2 - \frac{1}{\gamma} \|\Delta y\|^2 - 2\Delta z^\top \Lambda \Delta z - 2\Delta z^\top \Lambda (W \Delta z + U \Delta x) = \gamma \|\Delta x\|^2 - \frac{1}{\gamma} \|\Delta y\|^2 - 2\Delta z^\top \Lambda (\Delta z - \Delta v) \geq 0, \quad (26)$$

which further implies that (14) is γ -Lipschitz since

$$\gamma \|\Delta x\|^2 - \frac{1}{\gamma} \|\Delta y\|^2 \geq 2\Delta z^\top \Lambda (\Delta v - \Delta z) \geq 0$$

where the last inequality follows by Lemma A.1.

D.3. Proof of Theorem 3.2

Sufficient. We show that (19) holds with $\Lambda = \text{diag}(\Lambda_0, \dots, \Lambda_{L-1})$ where $\Lambda_k = \Psi_k^2$. Since the structure of H is a chordal graph, $H \succeq 0$ is equivalent to the existence of a chordal decomposition (Zheng et al., 2021):

$$H = \sum_{k=0}^L E_k H_k E_k^\top \quad (27)$$

where $0 \preceq H_k \in \mathbb{R}^{(n_k+n_{k+1}) \times (n_k+n_{k+1})}$ and $E_k = [\mathbf{0}_{a,k} \quad \mathbf{I}_{b,k} \quad \mathbf{0}_{c,k}]$ with $\mathbf{I}_{b,k}$ being the identity matrix the same size as H_k , and $\mathbf{0}_{a,k}, \mathbf{0}_{c,k}$ being zero matrices of appropriate dimension. We then construct H_k as follows.

For $k = 0$, we take

$$H_0 = \begin{bmatrix} \gamma I & -\sqrt{2\gamma} B_0^\top \Psi_0 \\ -\sqrt{2\gamma} \Psi_0 B_0 & 2\Psi_0 (I - A_0 A_0^\top) \Psi_0 \end{bmatrix}. \quad (28)$$

Note that $H_0 \succeq 0$ since $[H_0]_{11} = \gamma I \succ 0$, and the Schur complement to $[H_0]_{11}$ yields

$$2\Psi_0 (I - A_0 A_0^\top) \Psi_0 - \sqrt{2\gamma} \Psi_0 B_0 \frac{1}{\gamma} I \sqrt{2\gamma} B_0^\top \Psi_0 = 2\Psi_0 (I - A_0 A_0^\top - B_0 B_0^\top) \Psi_0 = 0.$$

For $k = 1, \dots, L-1$ we take

$$H_k = \begin{bmatrix} 2\Psi_{k-1} A_{k-1} A_{k-1}^\top \Psi_{k-1} & -2\Psi_{k-1} A_{k-1} B_k^\top \Psi_k \\ -2\Psi_k B_k A_{k-1}^\top \Psi_{k-1} & 2\Psi_k (I - A_k A_k^\top) \Psi_k \end{bmatrix}. \quad (29)$$

If A_{k-1} is zero, then it is trivial to have $H_k \succeq 0$. For nonzero A_{k-1} , we can verify that $H_k \succeq 0$ since the Schur complement to $[H_k]_{11}$ shows

$$\begin{aligned} & 2\Psi_k (I - A_k A_k^\top) \Psi_k - 2\Psi_k B_k A_{k-1}^\top \Psi_{k-1} (2\Psi_{k-1} A_{k-1} A_{k-1}^\top \Psi_{k-1})^+ 2\Psi_{k-1} A_{k-1} B_k^\top \Psi_k \\ &= 2\Psi_k (I - A_k A_k^\top - B_k B_k^\top) \Psi_k + 2\Psi_k B_k (I - A_{k-1}^+ A_{k-1}) B_k^\top \Psi_k \\ &= 2\Psi_k B_k (I - A_{k-1}^+ A_{k-1}) B_k^\top \Psi_k \succeq 0 \end{aligned}$$

where X^+ denotes the Moore–Penrose inverse of the matrix X , and it satisfies $I - X^+ X \succeq 0$.

For $k = L$ we take

$$H_L = \begin{bmatrix} 2\Psi_{L-1} A_{L-1} A_{L-1}^\top \Psi_{L-1} & -\sqrt{2\gamma} A_{L-1} B_L^\top \Psi_{L-1} \\ -\sqrt{2\gamma} \Psi_{L-1} B_L A_{L-1}^\top & \gamma I \end{bmatrix}. \quad (30)$$

Similarly, we can conclude $H_L \succeq 0$ using Schur complement

$$\gamma I - \sqrt{2\gamma} \Psi_{L-1} B_L A_{L-1}^\top (2\Psi_{L-1} A_{L-1} A_{L-1}^\top \Psi_{L-1})^+ \sqrt{2\gamma} A_{L-1} B_L^\top \Psi_{L-1} = \gamma \Psi_{L-1} B_L (I - A_{L-1}^+ A_{L-1}) B_L^\top \Psi_{L-1} \succeq 0.$$

We now show that H_k with $k = 0, \dots, L$ satisfy the chordal decomposition (27) holds since

$$\begin{aligned} [H_k]_{21} &= -2\Psi_k B_k A_{k-1}^\top \Psi_{k-1} = -\Psi_k^2 (2\Psi_k^{-1} B_k A_{k-1}^\top \Psi_{k-1}) = -\Lambda_k W_k, \\ [H_k]_{22} + [H_{k+1}]_{11} &= 2\Psi_k (I - A_k A_k^\top) \Psi_k + 2\Psi_k A_k A_k^\top \Psi_k = 2\Psi_k^2 = 2\Lambda_k. \end{aligned}$$

Finally, we conclude that $H \succeq 0$ from (Zheng et al., 2021)[Theorem 2.1].

Necessary. For any W_k and Λ_k satisfying (19), we will find set of free variables d_k, X_k, Y_k such that (7) holds. We take $\Psi_k = \Lambda_k^{\frac{1}{2}}$ which further leads to $d_k = \text{diag}(\log \Psi_k)$. By letting $A_{-1} = I, \Psi_{-1} = \sqrt{\gamma/2}I$ and $\Psi_L = \sqrt{2/\gamma}I$ we then construct A_k, B_k recursively via

$$B_k = \frac{1}{2}\Psi_k W_k \Psi_{k-1}^{-1} A_{k-1}^{-\top}, \quad A_k = \text{chol}(I - B_k B_k^\top) Q_k \quad (31)$$

where $\text{chol}(\cdot)$ denotes the Cholesky factorization, Q_k is an arbitrary orthogonal matrix such that A_k does not have eigenvalue of -1 . If A_{k-1} is non-invertible but non-zero, we replace $A_{k-1}^{-\top}$ with $(A_{k-1}^+)^{\top}$. If $A_{k-1} = 0$ (i.e. $W_k = 0$), we simply reset $A_{k-1} = I$. It is easy to verify that Ψ_k, A_k and B_k satisfy the model parameterization (7). Finally, we can construct X_k, Y_k using (36), which is well-defined as A_k does not have eigenvalue of -1 .

D.4. Proof of Theorem 3.3

The proposed layer (9) can be rewritten as a compact network (16) with $W = 0, Y = \sqrt{2}A^\top \Psi$ and $U = \sqrt{2}\Psi^{-1}B$, i.e.,

$$v = U h_{\text{in}} + b, \quad z = \sigma(v), \quad h_{\text{out}} = Y z.$$

From the model parameterization (6) we have $AA^\top + BB^\top = I$, which further implies

$$2\Psi^2 - Y^\top Y - \Psi^2 U U^\top \Psi^2 = 2\Psi^2 - 2\Psi A A^\top \Psi - 2\Psi B B^\top \Psi = 2\Psi(I - A A^\top - B B^\top)\Psi = 0$$

By applying Schur complement twice to the above equation we have

$$\begin{bmatrix} I & -U^\top \Psi^2 & 0 \\ -\Psi^2 U & 2\Psi^2 & -Y^\top \\ 0 & -Y & I \end{bmatrix} \succeq 0.$$

Then, the 1-Lipschitzness of (9) is obtained by Theorem A.3.

D.5. Proof of Proposition 3.5

Sufficient. It is a direct corollary of Theorem 3.3 by taking the identity operator as the nonlinear activation.

Necessary. Here we give a constructive proof. That is, given a weight matrix W with $\|W\| \leq 1$, we will find a (generally non-unique) pair of (X, Y) such that $2A^\top B = W$ with A, B given by (6).

We first construct A, B from W . Since it is obvious for $W = 0$, we consider the case with nonzero W . First, we take a singular value decomposition (SVD) of W , i.e. $W = U_w \Sigma_w V_w^\top$ where U_w is a $q \times q$ orthogonal matrix, Σ_w is an $q \times p$ rectangular diagonal matrix with $\Sigma_{w,ii} \geq 0$ non-increasing, V_w is a $p \times p$ orthogonal matrix. Then, we consider the candidates for A and B as follows:

$$A = U \Sigma_a U_w^\top, \quad B = U \Sigma_b V_w^\top \quad (32)$$

where Σ_a is a diagonal matrix, Σ_b a rectangular diagonal matrix $U \in \mathbb{R}^{q \times q}$ an orthogonal matrix. By substituting (32) into the equalities $AA^\top + BB^\top = I_q$ and $W = 2A^\top B$ we have

$$\Sigma_a^2 + \Sigma_{b'}^2 = I_q, \quad 2\Sigma_a \Sigma_{b'} = \Sigma_{w'} \quad (33)$$

where $\Sigma_{b'}, \Sigma_{w'} \in \mathbb{R}^{q \times q}$ are obtained by either removing the extra columns of zeros on the right or adding extra rows of zeros at the bottom to Σ_b and Σ_w , respectively. The solution to (33) is

$$\Sigma_{a,ii} = \frac{1}{2} \left(\sqrt{1 + \Sigma_{w',ii}} + \sqrt{1 - \Sigma_{w',ii}} \right), \quad \Sigma_{b',ii} = \frac{1}{2} \left(\sqrt{1 + \Sigma_{w',ii}} - \sqrt{1 - \Sigma_{w',ii}} \right) \quad (34)$$

where are well-defined as $\|W\| \leq 1$. Now we can obtain Σ_b from $\Sigma_{b'}$ by removing extra rows of zeros at the bottom or adding extra columns of zeros on the right. At last, we pick up any orthogonal matrix U such that $A = U \Sigma_a U_w^\top$ does not have eigenvalue of -1 .

The next step is to find a pair of (X, Y) such that

$$A^\top = (I + Z)^{-1}(I - Z), \quad B^\top = -2Y(I + Z)^{-1}, \quad Z = X - X^\top + Y^\top Y. \quad (35)$$

One solution to the above equation is

$$Z = (I - A^\top)(I + A^\top)^{-1}, \quad Y = -\frac{1}{2}B^\top(I + Z), \quad X = \frac{1}{2}\text{tril}(Z - Z^\top) \quad (36)$$

where $\text{tril}(W)$ denotes the strictly lower triangle part of W . Note that the above solution is well-defined since A does not has eigenvalue of -1 .

D.6. Proof of Proposition 3.6

From (28) we have

$$H_0 = \begin{bmatrix} \gamma I & -W_0^\top \Psi_0^2 \\ -\Psi_0^2 W_0 & 2\Psi_0 B_0 B_0^\top \Psi_0 \end{bmatrix} \succeq 0.$$

Applying the Schur complement yields $\gamma I - 1/2W_0^\top \Psi_0 (B_0 B_0^\top)^+ \Psi_0 W_0 \succeq 0$, which implies $\|B_0^+ \Psi_0 W_0\| \leq \sqrt{2\gamma}$. From (29) we obtain

$$\begin{aligned} H_k &= \begin{bmatrix} 2\Psi_{k-1} A_{k-1} A_{k-1}^\top \Psi_{k-1} & -W_k^\top \Psi_k^2 \\ -\Psi_k^2 W_k & 2\Psi_k B_k B_k^\top \Psi_k \end{bmatrix} \succeq 0 \\ \Rightarrow \Psi_{k-1} A_{k-1} A_{k-1}^\top \Psi_{k-1} - \frac{1}{4}W_k^\top \Psi_k (B_k B_k^\top)^+ \Psi_k W_k &\succeq 0 \\ \Rightarrow I - \frac{1}{4}A_{k-1}^+ \Psi_{k-1}^{-\top} W_k^\top \Psi_k (B_k B_k^\top)^+ \Psi_k W_k \Psi_{k-1}^{-1} (A_{k-1}^\top)^+ &\succeq 0 \\ \Rightarrow \left\| \frac{1}{2}B_k^+ \Psi_k W_k \Psi_{k-1}^{-1} (A_{k-1}^\top)^+ \right\| &\leq 1. \end{aligned}$$

Similarly, from (30) we have

$$H_L = \begin{bmatrix} 2\Psi_{L-1} A_{L-1} A_{L-1}^\top \Psi_{L-1} & -W_L^\top \\ -W_L & \gamma I \end{bmatrix} \succeq 0 \Rightarrow \|W_L \Psi_{L-1}^{-1} (A_{L-1}^\top)^+\| \leq \sqrt{2\gamma}.$$

The bound of $\mathbf{J}^c f$ is then obtained by

$$\begin{aligned} \|\mathbf{J}^c f\| &= \|W_L J_{L-1} W_{L-1} \cdots J_0 W_0\| \\ &= \left\| \frac{1}{2}W_L \Psi_{L-1}^{-1} (A_{L-1}^\top)^+ (2A_{L-1}^\top J_{L-1} B_{L-1}) \prod_{k=L-1}^1 \left(\frac{1}{2}B_k^+ \Psi_k W_k \Psi_{k-1}^{-1} (A_{k-1}^\top)^+ \right) (2A_{k-1}^\top J_{k-1} B_{k-1}) (B_0^+ \Psi_0 W_0) \right\| \\ &\leq (\sqrt{2\gamma})^2 / 2 = \gamma \end{aligned}$$

where the first inequality follows as $2A_k^\top J_k B_k$ is the Clarke Jacobian of a 1-Lipschitz layer (9), i.e. $\|2A_k^\top J_k B_k\| \leq 1$.

E. Training details

For all experiments, we used a piecewise triangular learning rate (Coleman et al., 2017) with maximum rate of 0.01. We use Adam (Kingma & Ba, 2014) and ReLU as our default optimizer and activation, respectively. Because the Cayley transform in (6) involves both linear and quadratic terms, we implemented the weight normalization method from (Winston & Kolter, 2020). That is, we reparameterize X, Y in $Z = X - X^\top + Y^\top Y$ by $g \frac{X}{\|X\|_F}$ and $h \frac{Y}{\|Y\|_F}$ with learnable scalars g, h . We search for the empirical lower Lipschitz bound $\underline{\gamma}$ of a network f_θ by a PGD-like method, i.e., updating the input x and its deviation δ_x based on the gradient of $\|f_\theta(x + \Delta x) - f_\theta(x)\|/\|\Delta x\|$. As we are interested in the global lower Lipschitz bound, we do not project x and $x + \Delta x$ into any compact region. For image classification tasks, we applied data augmentation used by (Araujo et al., 2023). All experiments were performed on an Nvidia A5000.

Toy example. For the curve fitting experiment, we take 300 and 200 samples (x_i, y_i) with $x_i \sim \mathcal{U}([-2, 2])$ for training and testing, respectively. We use batch size of 50 and Lipschitz bounds of 1, 5 and 10. All models for the toy example have 8 hidden layers. We choose width of 128, 128, 128 and 86 for AOL, orthogonal, SLL and sandwich layers, respectively, so that each model size is about 130K. We use MSE loss and train models for 200 epochs.

Table 4. Model architectures for MNIST.

MLP	Orthogonal	Sandwich
Fc (784, 256)	OgFc (784, 256)	SwFc (784, 190)
Fc (256, 256)	OgFc (256, 256)	SwFc (190, 190)
Fc (256, 128)	OgFc (256, 128)	SwFc (190, 128)
Lin (128, 10)	OgLin (128, 10)	SwLin (128, 10)

Table 5. Model architectures for CIFAR-10/100 and Tiny-ImageNet. We use $w = 1, 2, 4$ to denote the *small, medium* and *large* models. The default kernel size for all convolution is 3. For orthogonal and sandwich convolution, we use the emulated 2-stride from (Trockman & Kolter, 2021) when $s=2$ is indicated. For CNN, $s=2$ refers to the standard 2-stride operation. Since the AOL layer does not support stride operation, we add average pooling at the end to convolution layers. Here `ncls` denotes the number of classes in the dataset, e.g. 100 for CIFAR-100 and 200 for Tiny-ImageNet.

CNN	AOL	Orthogonal	Sandwich
Conv (3, 32*w)	AolConv (3, 32*w)	OgConv (3, 32*w)	SwConv (3, 32*w)
Conv (32*w, 32*w, s=2)	AolConv (32*w, 32*w)	OgConv (32*w, 32*w, s=2)	SwConv (32*w, 32*w, s=2)
Conv (32*w, 64*w)	AolConv (32*w, 64*w)	OgConv (32*w, 64*w)	SwConv (32*w, 64*w)
Conv (64*w, 64*w, s=2)	AolConv (64*w, 64*w)	OgConv (64*w, 64*w, s=2)	SwConv (64*w, 64*w, s=2)
Flatten	AvgPool (4), Flatten	Flatten	Flatten
Fc (4096*w, 640*w)	AolFc (4096*w, 640*w)	OgFc (4096*w, 640*w)	SwFc (4096*w, 512*w)
Fc (640*w, 512*w)	AolFc (640*w, 512*w)	OgFc (640*w, 512*w)	SwFc (512*w, 512*w)
Lin (512*w, ncls)	AolLin (512*w, ncls)	OgLin (512*w, ncls)	SwLin (512*w, ncls)

Image classification. We trained small fully-connected model on MNIST and the KWLARGE network from (Li et al., 2019) on CIFAR-10. To make the different models have similar number of parameters in the same experiment, we slightly reduce the hidden layer width of sandwich model in the MNIST experiment and increases width of the first fully-connected layer of CNN and orthogonal models. The model architectures are reported in Table 4 - 5. We used the same loss function as (Trockman & Kolter, 2021) for MNIST and CIFAR-10 datasets. The Lipschitz bounds are chosen to be 0.1, 0.5, 1.0 for MNIST and 1, 10, 100 for CIFAR-10. All models are trained with normalized input data for 100 epochs. For the experiment of empirical robustness, model architectures with different sizes are reported in Table 5. The SLL model with small, medium and large size can be found in (Araujo et al., 2023). We train models with different Lipschitz bounds of $\{0.5, 1, 2, \dots, 16\}$. We found that $\gamma = 2$ for CIFAR-100 and $\gamma = 1$ for Tiny-ImageNet achieve the best robust accuracy for the perturbation size of $\epsilon = 36/255$. Note that the effective model Lipschitz bound is 4 times larger due to input data normalization. We also compare the certified robustness to the SLL model. Slightly different from the experimental setup for empirical robustness comparison, we remove the data normalization and use the Last Layer Normalization (LLN) proposed by (Singla et al., 2022) which can improve the certified accuracy when the number of classes becomes large. We set the Lipschitz bound of sandwich and SLL models to 1. But the Lipschitz constant of the composited model could be larger than 1 due to LLN. Due to LLN. The certified accuracy is then normalized by the last layer (Singla et al., 2022). Also, we remove the data normalization for better certified robustness. For all experiments on CIFAR-100 and Tiny-ImageNet, we use the CrossEntropy loss as in (Prach & Lampert, 2022) with temperature of 0.25 and an offset value $3\sqrt{2}/2$.

Table 6. Sandwich models in the experiment of certified robustness. Here `LLN` stands for the Last Layer Normalization (Singla et al., 2022) which can improve the certified robustness when the number of classes become large.

CIFAR-100	TinyImageNet
SwConv (3, 64)	SwConv (3, 64)
SwConv (64, 64, s=2)	SwConv (64, 64, s=2)
SwConv (64, 128)	SwConv (64, 128)
SwConv (128, 128, s=2)	SwConv (128, 128, s=2)
SwConv (128, 256)	SwConv (128, 256)
SwConv (256, 256, s=2)	SwConv (256, 256, s=2)
-	SwConv (256, 512)
-	SwConv (512, 512, s=2)
SwFc (1024, 2048)	SwFc (2048, 2048)
SwFc (2048, 2048)	SwFc (2048, 2048)
SwFc (2048, 1024)	SwFc (2048, 1024)
LLN (1024, 100)	LLN (1024, 200)